

Stochastic modeling framework for polymer bonding based on classical physics and
chemical bonding model

Vas L. M., Tóth Cs., Petrény R., Virág Á. D.

Accepted for publication in Applied Physics A: Materials Science and Processing

Published in 2025

DOI: <https://doi.org/10.1007/s00339-025-08971-4>



Stochastic modeling framework for polymer bonding based on classical physics and chemical bonding model

László Mihály Vas¹ · Csenge Tóth^{1,2} · Roland Petrényi¹ · Ábris Dávid Virág¹

Received: 21 July 2025 / Accepted: 16 September 2025
© The Author(s) 2025

Abstract

In this article, we present a unified stochastic framework that models both primary (covalent) and secondary (noncovalent) bonding in polymers by mapping electron-residence probabilities onto classical potentials. From simple probabilistic assumptions together with Coulombic and a modified Lennard–Jones functional form, we derive closed-form, distance-dependent expressions for bond energies and forces and space correlation function that are directly usable in atomistic simulations. Validation on O–H interactions in polylactic-acid hydrolysis yields excellent agreement with detailed force-field calculations at a small fraction of the computational cost. The analytic, low-parameter nature of the approach facilitates rapid incorporation of physics-based bond descriptions into kinetic, continuum, and multiscale polymer modeling workflows and is naturally extensible with lightweight data-driven corrections.

Keywords Electron residence probability · Electronegativity · Lennard-Jones potential · Dipole · Hydrogen bond

1 Introduction

The physical and chemical properties of polymer materials are influenced by the atoms they contain and the primary and secondary bonds between them. Bonding type and strength between different atoms has been one of the most researched areas of physics and materials science and has been the subject of many models over the last century [1]. The primary or secondary bonds between two atoms or molecules are determined by the probability of the electrons being in the vicinity of one or the other nucleus [2].

There are several simplified models for different types of primary bonds specific to the type of bond. Covalent bonds are formed when atoms share electrons. Ionic bonds occur when atoms transfer electrons, which

gives an asymmetric probability density of electrons in a molecule, while metallic bonds involve a relatively uniform probability density of electrons over a lattice of positively charged ions [3, 4]. The Lewis theory of bonding can be applied to describe covalent and ionic bonds, representing bonds as electron pairs shared or transferred between atoms to achieve stable electron configurations without describing bonding through orbital overlap [5]. Valence Bond (VB) Theory provides a more detailed, quantum-mechanical approach that explains bond strength, orbital overlap, and molecular geometry [6]. According to VB theory, a bond between two atoms is created by overlapping the half-filled valence orbitals of the two atoms containing an unpaired electron. Due to the overlap, the electrons are most likely to be in the space around the bond [7–9].

The van Arkel–Ketelaar triangles of bonding is a generally applicable, simplified model to describe how and which type of bond is formed between two atoms. This graphical representation is used to visualize the type of bonding (ionic, covalent, or metallic) in binary chemical compounds using only the electronegativities of the constituent atoms. Based on the average electronegativity of the constituents on the x-axis and the electronegativity difference on the y-axis, the dominantly formed bond between the constituents can be predicted. The upper tip

✉ Roland Petrényi
petrenyr@pt.bme.hu

¹ Department of Polymer Engineering, Faculty of Mechanical Engineering, Budapest University of Technology and Economics, Műegyetem rkp. 3, Budapest H-1111, Hungary

² MTA-BME Lendület Lightweight Polymer Composites Research Group, Budapest University of Technology and Economics, Műegyetem rkp. 3, Budapest H-1111, Hungary

of the triangle indicates the formation of ionic bonds due to the large electronegativity difference, the lower right tip indicates the formation of covalent bonds due to the large average and small difference in electronegativity, while the lower left tip indicates a delocalized electron cloud, a metallic bond, due to the small difference and small average [10–12]. Recent studies have also shown how understanding bonding interactions and electronic structure is essential for interpreting charge transport and recombination processes in functional organic materials [13, 14].

Modern quantum mechanics describes the aforementioned behavior using wave functions, which determine the probability density of finding an electron in a particular region around the nucleus. An analytical solution of this is the Schrödinger equation, which provides the wave function as a solution, and in turn, gives the probability distribution of electron positions [15]. The square of the absolute value of the wave function gives the probability density function of finding the electron in the vicinity of a particular point in space [16]. *Ab initio* methods, such as the Density Functional Theory (DFT) and the Hartree-Fock method, rely directly on fundamental quantum mechanical principles without empirical parameters. The DFT is used to study the electronic structure of many-body systems, particularly atoms, molecules, and solids, by describing the system's energy in terms of electron density rather than wavefunctions. It is widely applied in materials science and chemistry for predicting molecular properties, bonding behavior, and reactions at an atomic scale [17]. The Hartree-Fock method is used to solve the Schrödinger equation for many-electron systems, considering electron interactions in an averaged manner and neglecting electron correlation. It provides a foundational approach to understanding molecular orbitals and energies [18]. For complex systems, where analytical solutions are not feasible, Monte Carlo Simulations can approximate the probability distribution of electron positions, which involves generating random samples of electron positions according to a given probability distribution [19]. Another method that is commonly used in practice is Bader's Quantum Theory of Atoms in Molecules (QTAIM) which describes how atoms within a molecule behave and interact based on their electron density distributions. Its biggest advantage is that it is effective to investigate not only the atom-atom interactions such as the covalent or ionic bonds but also the non-covalent interactions like the van der Waals or hydrogen bonding. However, calculating the electron density with sufficient accuracy, especially for large molecules or systems, requires advanced quantum

chemical computations, which can be computationally expensive and time-consuming [20, 21].

The probability of the electrons in a molecule being in the vicinity of one or another atom determines not only the primary but also the secondary bonds [4, 22]. Secondary bonds are caused by temporary fluctuations or permanent asymmetries in electron density, creating dipoles. If the electron density fluctuates temporarily, a dispersion bond is formed; in some literature, this bond is also called a van der Waals bond, but in this paper, we use the term dispersion bond for clarity. Dipole-dipole bonds are formed when there is a higher probability of electrons occurring around one atom than around the other. The hydrogen bond is a special case of dipole bonds, which occur between a hydrogen atom in one molecule and an electronegative atom in another. In this case, the electron of the hydrogen atom can be found in the vicinity of the other, highly electronegative atom, resulting in a strong asymmetry in electron density [4, 23].

Quantum-mechanical treatments of chemical bonding provide high fidelity but are often analytically intractable and computationally expensive, limiting their routine use in engineering workflows. Classical alternatives such as empirical force fields, quantum Monte Carlo, or topological analyses (e.g., QTAIM) reduce cost but still demand substantial parameterization effort, specialized software, and can fail to capture important electronic reorganization effects. This gap motivates a lightweight, interpretable surrogate that preserves the essential physics of electron sharing while remaining inexpensive and easy to integrate into existing simulation pipelines. We therefore propose an electron-residence-probability (ERP) framework that maps simple, distance-dependent probabilistic models onto functional forms to estimate the likelihood of electron localization between atom pairs. The ERP formulation requires few input parameters, incurs minimal computational overhead, and yields a transparent, physically motivated approximation that is directly useful to chemical and materials engineers for rapid exploration and for guiding more expensive quantum calculations. Augmenting ERP with a compact neural network [24, 25]—used either to predict parameters or to provide a residual energy correction trained with weighted energy/force losses and constrained by equivariant/invariant representations and physics-based clipping—produces a physics-informed, interpretable, and data-efficient hybrid. This combined model recovers missing induction and angular effects, improves fidelity relative to pure empirical forms, and delivers substantial speedups compared with *ab initio* methods, making it

well suited for multiscale and machine-learning-driven studies.

Notation	
Symbol	Definition
a, b, c	constants of the correlation function
c_1, c_2	fitting constants of the formula for the ERP
f	normalized interactive force
g	product of the dipole end charges
h	trend function for the ϕ_i - p_i relationship
k	constant of the Coulomb's law
n, m	exponents of the Lennard-Jones potential function
p_i ($i=1, 2$)	electron residence probability (ERP) of the i^{th} atom or dipole end
$p_{i,j}$	joint probability for the electron numbers at the independent dipole ends
$\hat{p}^{i,j}$	joint probability for the interacting dipole ends
$q = \text{abs}(E(\delta'))$	virtual random variable for $p=p_i$
$q_{n,k}$	average absolute charge of the dipole
$q_{2,j}$	probability that k electrons from n are in the vicinity of atom 1
r	marginal probabilities in the case of interacting dipole ends
r_0	distance between the ends of two dipoles
r^*	bond length (covalent or secondary bond)
$w_{i,j}$	distance to the maximum interaction force in the dipole
	transformation weight for the joint probability $P_{i,j}$
$\text{Cov}(Y_1, Y_2)$	covariance of stochastic variables Y_1 and Y_2
C_{y_1, y_2}	empirical covariance of y_1 and y_2 values
$\text{CV}(Y)$	coefficient of variation of stochastic variable Y
$\mathbf{D}(Y)$	standard deviation of stochastic variable Y
$\text{DI} = \text{abs}(E(\delta))$	Dipole Index
$E(Y)$	Expectation of stochastic variable Y
EN	Electronegativity
EN_i ($i=1, 2$)	Electronegativity of the i^{th} atom
F	interactive force between dipole ends
$F_0 = \text{abs}(F(r_0))$	maximum of the interactive force
G	expectation of g
G_0	value of G when $r=r_0$
G_∞	limit value of G
M	metal
NM	non-metal
$\mathbf{P}(A)$	Probability of event A
Q_e	electron charge
Q_i ($i=1, 2$)	electric charge of the i^{th} dipole end in general
$R(Y_1, Y_2)$	correlation coefficient of stochastic variables Y_1 and Y_2
R_{y_1, y_2}	empirical correlation coefficient of y_1 and y_2 values
RMSE	Relative Mean Squared Error
S_y	empirical standard deviation of given y values
U	potential energy (atom or dipole pair)
U_0	bond energy (covalent or secondary bond)
$W_{i,j}$	normalized transformation weight of $p_{i,j}$
X_i ($i=1, 2$)	state variable (number of electrons in the vicinity of the i^{th} atom or dipole end)
\bar{y}	arithmetic mean of given y values

Notation	
Symbol	Definition
α, β	constants of the Lennard-Jones (LJ) potential function
$\alpha_{m, n}$	ratio formed from the LJ-exponents
δ'	instantaneous dipole charge
$\delta = \delta'/Q_e$	normalized dipole charge
δ_i ($i=1, 2$)	relative charge of/about the i^{th} atom
ϵ_0	electric permittivity of free space (vacuum)
ϕ_i ($i=1, 2$)	electronegativity ratio of the i^{th} atom
ξ_i ($i=1, 2$)	fitted constant coefficients
ΔEN	absolute difference of electronegativities
ΣEN	sum of electronegativities
Ω	product of known and fitted parameters proportional with Ω_0
Ω_0	product of known (measured) parameters containing $r_0 U_0$

2 Theoretical considerations

2.1 Electron residence probability-based model of dipoles

To keep the mathematical description simple, in the present model, the electrons are not treated as quantum objects, but according to the classical physical approach, the electron is considered as an electrically charged particle with random position in the space, which can be characterized by the orbital provided by the time-independent Schrödinger equation, while any time-dependent properties of the electrons are ignored. A pair of atoms connected by a covalent bond forms a dynamic dipole with a continuously changing charge distribution (stochastic dipole process), in which electron pairs usually produce a common electron cloud [2, 7, 12, 26]. In a dynamic dipole, the surroundings of a single atom can be defined as a half-space, which is determined by a separation plane between the two covalent-bonded atoms, which is perpendicular to the straight line determined by the center points of the atoms [27]. In order to keep the demonstration simple, we assume that the electron resides in one half-space with a certain probability. i.e. at any arbitrary moment, the so called residence probability of an electron being in the spatial domain of the i -th atom (which is a half-space) is $0 \leq p_i \leq 1$, where $p_1 + p_2 = 1$ ($i=1, 2$). The dipole can be in one of three states at a given moment, according to the possible charge distributions of the electron pair in the spatial domain of the two atoms:

- (2,0) Both electrons are in the vicinity of atom 1, so an excess of 1 electron makes this side of the dipole negative, while the other is positive;
- (1,1) Each electron is in the vicinity of a different atom, therefore both sides of the dipole are neutral;

- (0,2) Both electrons are in the vicinity of atom 2, so this side of the dipole is negatively charged and the other positively charged.

The state of a dipole changes over time, and the momentary dipoles form a random stationary dipole flow. The state of a dipole can be described by the half-space electron residence probabilities (ERP: p_1 and p_2), and the average charge ($-q/+q$) of the dipole. The product of the average charge ($0 \leq q = E(\delta') \leq Q_e$, δ' is the momentary charge) and bond length (r_0) (which is the distance between the two atoms) is the dipole moment. In Eq. 1, we define the dipole index (DI), which equals to the absolute value of the average charge of the dipole normalised by the electron charge (Q_e), therefore DI can be considered the relative polarity of the dipole [28]. Moreover, the DI is also equal to the absolute value of the expectation ($|E(\delta)|$) of the relative momentary charge distribution ($\delta = \delta'/Q_e$).

$$0 \leq DI = \left| \frac{qr_0}{Q_e r_0} \right| = \left| \frac{q}{Q_e} \right| = \left| \frac{E(\delta')}{Q_e} \right| = |E(\delta)| \leq 1, \quad \delta = \frac{\delta'}{Q_e} \quad (1)$$

If $DI = 0$, then the two atoms are identical or at least have the same electronegativity (EN), therefore the bond is apolar on average. In this case, $p_1 = p_2$ and the probability of the dipole states (2;0) and (0;2) are equal. If $DI > 0$, then the two atoms differ in EN and the bond is polar on average (for e.g. if $EN_1 > EN_2$ then $p_1 > p_2$). In the former case, the atoms form momentary dipoles only, while in the latter case, they form permanent dipoles. Depending on the degree of DI, the permanent dipole can be weakly or strongly polarised.

Assuming that the electrons in a covalent bond are independent of each other, the states of the diatomic system can be described by a binomial probability model [29, 30]. If the state variable, X_i equals the number of common electrons (0,1,2) in the vicinity of the i -th atom ($i = 1, 2$), and p_i is the probability that a given electron resides at the vicinity of the i -th atom, which is the electron residence probability (ERP) (Fig. 1), then the

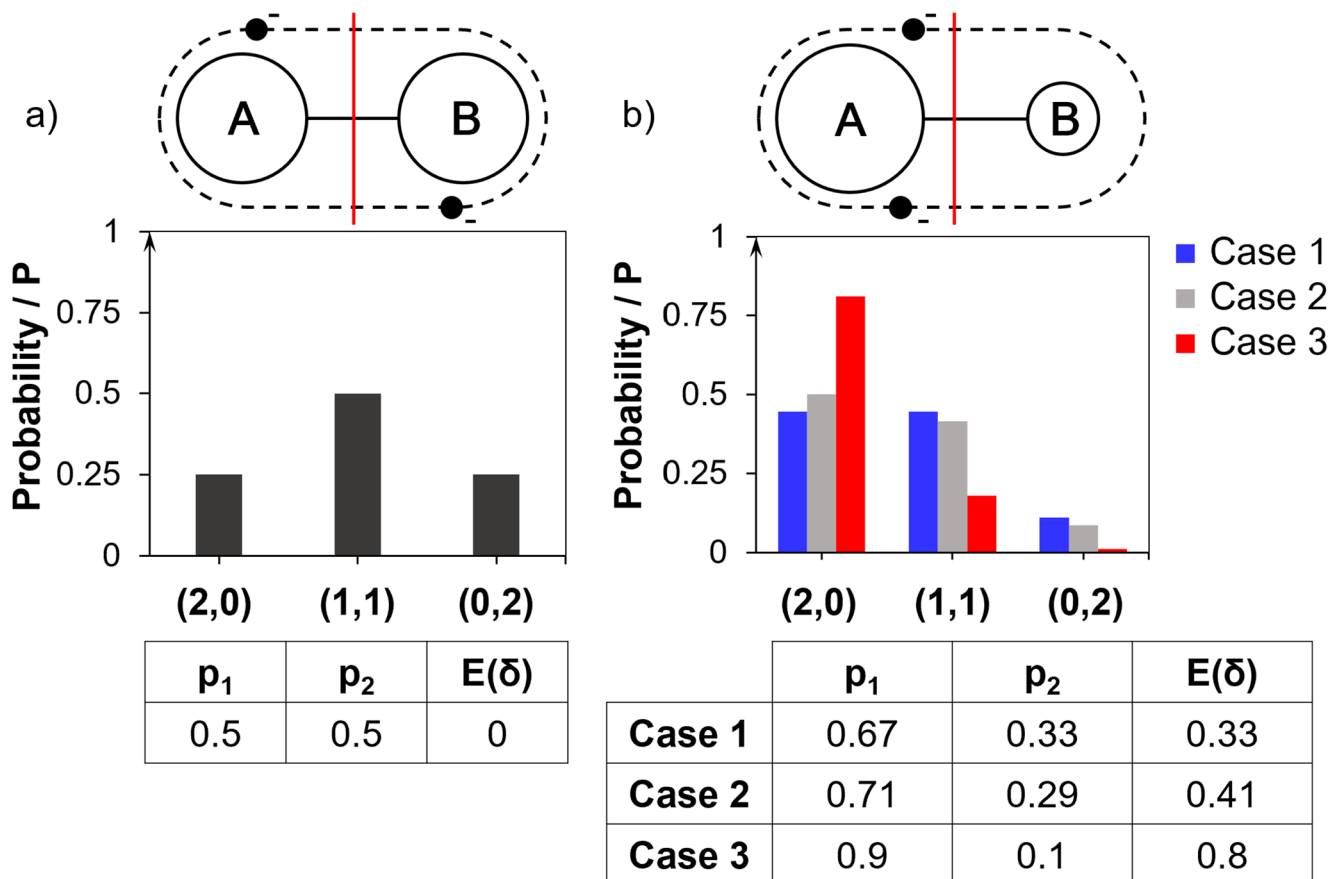


Fig. 1 Characterization of covalent bonds with electron residence probabilities (ERP) in a diatomic system: momentary (a) and quasi-permanent dipole (b). The notation on the x-axis denotes the electron distribution between the two half-spaces: the first number in parenthe-

ses corresponds to the number of electrons in the left half-space, and the second number corresponds to the number of electrons in the right half-space (e.g., (2,0) indicates 2 electrons in the left half-space and 0 in the right)

probability (**P**) that there are *k* electrons in the vicinity of the 1st atom 1 (*k* = 0,1,2) and *n* - *k* electrons in the vicinity of 2nd atom is described by Eq. 2:

$$q_{n,k} = P(X_1 = k, X_2 = n - k) = \binom{n}{k} p_1^k (1 - p_1)^{n-k} \quad (2)$$

where *n* is the possible maximum number of the shared electrons. Theoretically, $0 < n \leq 8$ and $0 \leq X_i \leq n$. However, note that quadruple covalent bonds are extremely rare and mostly, $0 < n \leq 6$. If the momentary relative charge of the *i*th (*i* = 1, 2) atom in the diatomic dipole is δ_i (= -1, 0, 1), it can be expressed by the state variable (Eq. 3).

$$\delta_i = 1 - X_i, \quad \delta_1 + \delta_2 = 0 \quad (3)$$

Thus the expected charge of the 1st ($\delta = \delta_1$) and 2nd ($\delta = \delta_2$) atom can be expressed as:

$$\begin{aligned} E(\delta_1) &= \sum_{k=0}^2 \delta_k q_{2,k} = 1 \cdot q_{2,0} + 0 \cdot q_{2,1} + (-1) \cdot q_{2,2} \\ &= 1 - 2p_1 \Rightarrow E(\delta_2) = -E(\delta_1) = 2p_1 - 1 = 1 - 2p_2 \end{aligned} \quad (4)$$

Whose absolute value is the dipole index: $DI = |E(\delta)| = |E(\delta_i)|$ (*i* = 1, 2).

For an apolar covalent bond, $p_1 = p_2 = 1/2$. Therefore, the state probabilities give a symmetric distribution, where $DI = E(\delta) = 0$. The probability of the formation of a neutral state and instantaneous dipoles is $q_{1,1} = P(1,1) = 0.5$ and $q_{2,0} = P(2,0) = q_{0,2} = P(0,2) = 0.25$, respectively (Fig. 1/a). If $p_1 = 1$, the atoms form an ideal permanent dipole, the ideal ionic bond ($DI = 1$). Some examples of the states between the aforementioned two extremes are shown in Fig. 1/b.

For double or triple covalent bonds, the number of electron pairs can be 4 or 6, respectively. As the number of electron pairs increases, the state probabilities of an apolar dipole remain symmetrically distributed, but the probability of a neutral instantaneous state decreases (Fig. 2/a-c).

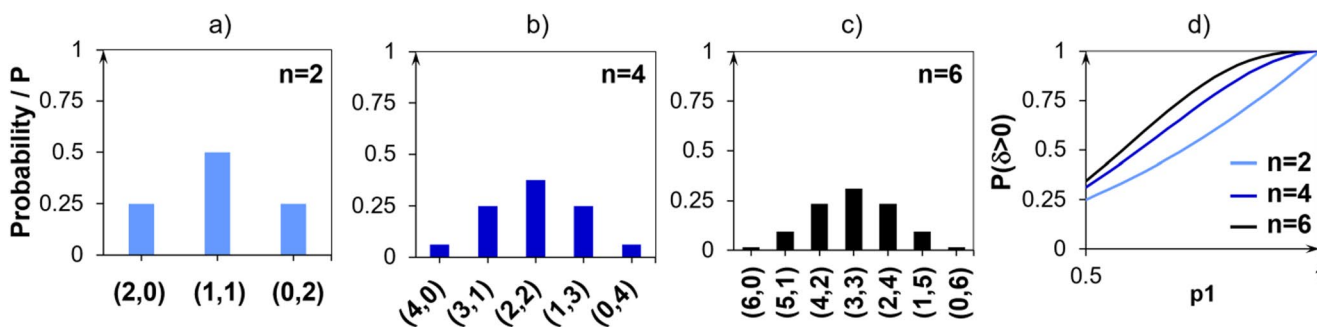


Fig. 2 State probabilities of an apolar dipole for 2 (a) 4 (b) and 6 electrons (c) and dipole probabilities (**P**) as a function of electron residence probability (*p*₁) for *n* = 2, 4, and 6 electrons (d). In a–c), the notation on the x-axis denotes the electron distribution between the two half-

spaces: the first number in parentheses corresponds to the number of electrons in the left half-space, and the second number corresponds to the number of electrons in the right half-space (e.g., (3,1) indicates 3 electrons in the left half-space and 1 in the right)

2.2 Stochastic model of dipole pairs and secondary bonds

The relationship between two dipoles can also be described using the electron residence probability-based (ERP-based) model of the dipole. For the simpler mathematical description, we consider the facing dipole-ends as Q_1 and Q_2 charged particles, and attractive (+) or repulsive (-) force arises between them at a distance of $r > 0$ [31]. Neglecting other dynamic effects, the relationship between two dipoles can be described by Coulomb’s law as a point-point interaction according to Eq. 5 (see the Supplementary material). In this approach, Eq. 5 does not take into account the relative orientation of the dipoles. In dynamic systems, the orientation fluctuates due to thermal motion and external fields, potentially affecting the attractive or repulsive forces and leading to deviations from Coulomb-based estimations [32].

$$F(r, t) = -k \frac{Q_1(r, t) Q_2(r, t)}{r^2} \xrightarrow{r \rightarrow \infty} 0 \quad (5)$$

In our case, at fixed *r* value, both charges change in time (*t*) and these changes are independent. There is no interaction between them if *r* is large enough. As they get closer, their resultant interaction is attractive, which becomes stronger. The attractive/repulsive force between them is at its maximum when both dipole ends have a maximum or a minimum charge. This means that if there is an electron excess (-) or deficit (+) of 1 electron at each end, the repulsion force is at its maximum ($|Q_1 Q_2| \leq Q_e^2$). Similarly, the attraction force is at its maximum ($Q_1 Q_2 = -Q_e^2$), when there is an electron surplus at one end and an electron deficit at the other

(Fig. 1/b). The force between these charges (F_θ) is therefore the strongest attractive/repulsive force in the dipole pair in absolute value, which occurs when $r=r_\theta$, where r_θ is the (secondary) bond distance. Normalising Eq. 5 by $F_0 = |F(r_\theta)|$, we obtain the signed product of the relative dipole charges (δ_i) and the distance coefficient (where $r_\theta \leq r$) (Eq. 6):

$$f(r, t) = \frac{F(r, t)}{F_0} = -\frac{Q_1(r, t) Q_2(r, t) r_0^2}{Q_e^2 r^2} = -\delta_1(r, t) \delta_2(r, t) \frac{r_0^2}{r^2} = g(r, t) \frac{r_0^2}{r^2} \leq 1 \tag{6}$$

At fixed r value, the expected value of $f(r, t)$ depends on the stochastic interaction, which can be described by the covariance and correlation of δ_1 and δ_2 (Eq. 7):

$$\begin{aligned} \bar{f}(r) &= \mathbf{E}(f(r, t)) = -\mathbf{E}(\delta_1(r, t) \delta_2(r, t)) \frac{r_0^2}{r^2} = \mathbf{E}(g(r, t)) \frac{r_0^2}{r^2} \\ &= -[\text{Cov}(\delta_1(r, t), \delta_2(r, t)) + \mathbf{E}(\delta_1(r, t)) \mathbf{E}(\delta_2(r, t))] \frac{r_0^2}{r^2} \\ &= -\mathbf{E}(\delta_1) \mathbf{E}(\delta_2) \left[\frac{\text{Cov}(\delta_1(r, t), \delta_2(r, t))}{\mathbf{D}(\delta_1) \mathbf{D}(\delta_2)} \frac{\mathbf{D}(\delta_1) \mathbf{D}(\delta_2)}{\mathbf{E}(\delta_1) \mathbf{E}(\delta_2)} + 1 \right] \frac{r_0^2}{r^2} \\ &= -\mathbf{E}(\delta_1) \mathbf{E}(\delta_2) \bullet [1 + R(\delta_1, \delta_2) CV(\delta_1) CV(\delta_2)] \frac{r_0^2}{r^2} \xrightarrow{r \rightarrow \infty} 0 \end{aligned} \tag{7}$$

where $g(r, t)$ is defined by Eqs. 6 and 7, and $\mathbf{D}(\delta_i)$ and $CV(\delta_i) = \mathbf{D}(\delta_i)/\mathbf{E}(\delta_i)$ are the standard deviation and the coefficient of variation of δ_i , respectively. Using Eq. 3 and the definition of covariance (Cov) and the correlation coefficient (R), we obtain [29, 30, 33]:

$$Cov(\delta_1, \delta_2) = \mathbf{E}[(\delta_1 - \mathbf{E}(\delta_1))(\delta_2 - \mathbf{E}(\delta_2))] = Cov(X_1, X_2) \tag{8}$$

$$R(\delta_1, \delta_2) = \frac{Cov(\delta_1, \delta_2)}{\mathbf{D}(\delta_1) \mathbf{D}(\delta_2)} \tag{9}$$

The expectation by Eq. 7 tends to zero when the distance, r , tends to infinity. For negligibly interacting dipole ends that are far apart, covariance is zero. The interaction between the dipole ends (Eq. 7) is generated by the common electrons of the pairs of atoms forming the dipole. Therefore, it can be assumed that the expected value of the $f(r, t)$ force increases (in absolute terms) as the dipole ends come closer. This is analogous to the phenomenon within dipoles in covalent bonding, where the attractive forces between ionised atoms and the common electron cloud are balanced by repulsive forces between non-bonding electron shells. Accordingly, the charge distributions of the approaching dipole ends change in such a way that they mutually induce/synchronise each other. This process leads to an increasing dominance of attractive forces, which could be described by an increase in the correlation between the states of the two dipoles.

Due to independence, when the dipoles are distant enough, the probability of the state of a pair of dipoles (ij) in the far position can be calculated as the product of two binomial probabilities $q_{2,i}$ and $q_{2,j}$ ($i, j=0, 1, 2$) (Eq. 10):

$$\begin{aligned} p_{i,j} &= \mathbf{P}(X_1 = i, X_2 = j) = \mathbf{P}(\delta_1 = 1 - i, \delta_2 = 1 - j) \\ &= \mathbf{P}(X_1 = i) \mathbf{P}(X_2 = j) = q_{2,i} q_{2,j} \\ &= \left[\binom{2}{i} p_1^i (1 - p_1)^{2-i} \right] \left[\binom{2}{j} p_2^j (1 - p_2)^{2-j} \right] \end{aligned} \tag{10}$$

where we took into account Eq. 3 as well. Otherwise, $q_{2,i}$ and $q_{2,j}$ are the marginal probabilities of the joint probability p_{ij} . As the dipoles get closer, the interaction gets stronger, the probability keeps changing and the dipole charges depends more and more on the other dipole. Hence, the probability of repulsive effects decreases and the probability of attractive effects increases, making the distribution of state probabilities increasingly asymmetric. This dependency can be analysed with conditional probabilities:

$$\begin{aligned} \hat{p}_{i,j} &= \mathbf{P}(X_1 = i, X_2 = j) = \mathbf{P}(\delta_1 = 1 - i, \delta_2 = 1 - j) \\ &= \mathbf{P}(X_1 = i | X_2 = j) \mathbf{P}(X_2 = j) = \mathbf{P}(X_2 = j | X_1 = i) \mathbf{P}(X_1 = i) \end{aligned} \tag{11}$$

This interaction can be interpreted as a distribution transformation. Hence, it can be characterized by a $\{w_{ij}\}$ weight distribution multiplier ($0 \leq w_{ij}$) as follows (Eq. 12):

$$1 = \sum_{i,j=0}^2 p_{i,j} \text{Interaction} \sum_{i,j=0}^2 \hat{p}_{i,j} = 1, \quad \hat{p}_{i,j} = \frac{w_{i,j} p_{i,j}}{\sum_{i,j=0}^2 w_{i,j} p_{i,j}} \tag{12}$$

Based on Eqs. 11 and 12, the conditional probabilities may be given as follows [29, 30]:

$$\begin{aligned} \hat{p}_{i,j} &= \mathbf{P}(X_1 = i | X_2 = j) \mathbf{P}(X_2 = j) \\ &= W_{i,j} \mathbf{P}(X_1 = i) \mathbf{P}(X_2 = j) = W_{i,j} p_{i,j} \end{aligned} \tag{13}$$

$$\begin{aligned} \hat{p}_{i,j} &= \mathbf{P}(X_2 = j | X_1 = i) \mathbf{P}(X_1 = i) \\ &= W_{j,i} \mathbf{P}(X_2 = j) \mathbf{P}(X_1 = i) = W_{j,i} p_{i,j} \end{aligned} \tag{14}$$

therefore

$$\begin{aligned} W_{i,j} &= \frac{w_{i,j}}{\sum_{i,j=0}^2 w_{i,j} p_{i,j}} \\ &= \frac{\mathbf{P}(X_1 = i, X_2 = j)}{\mathbf{P}(X_1 = i) \mathbf{P}(X_2 = j)} \\ &= \frac{w_{j,i}}{\sum_{i,j=0}^2 w_{j,i} p_{i,j}} = W_{j,i} \end{aligned} \tag{15}$$

Hence, we may take that

$$w_{i,j} = w_{j,i} \tag{16}$$

Based on the formulae above, we can calculate the marginal probabilities $\hat{q}_{2,i}$ and $\hat{q}_{2,j}$ of the transformed joint probabilities $\hat{p}_{i,j}$:

$$\hat{q}_{2,i} = \sum_{j=0}^2 W_{i,j} p_{i,j}; \quad \hat{q}_{2,j} = \sum_{i=0}^2 W_{i,j} p_{i,j} \tag{17}$$

Being aware of the marginal probabilities allows us to determine the marginal expectations and standard deviations.

2.3 The interactive forces in the dipoles

The potential energy of a diatomic system can be approximated by the Lennard-Jones potential (Eq. 18) [2, 3, 26]:

$$U(r) \approx -\frac{\alpha}{r^m} + \frac{\beta}{r^{12}} = U_0 \left[\frac{m}{n-m} \left(\frac{r_0}{r}\right)^n - \frac{n}{n-m} \left(\frac{r_0}{r}\right)^m \right] \sim -\frac{nU_0}{n-m} \left(\frac{r_0}{r}\right)^m \xrightarrow{r \rightarrow \infty} 0 \quad (18)$$

$$r_0 = \left(\frac{n\beta}{m\alpha}\right)^{\frac{1}{n-m}}, \quad U_0 = \frac{\alpha(n-m)}{nr_0^m} = -U(r_0) \quad (19)$$

where α , β are positive constants, $m=6$, $n=12$ are integer exponents, r_0 is the bond distance and U_0 is the dissociation energy of the system. The resultant force between the two atoms can be obtained by differentiating $U(r)$:

$$F(r) = F_{att}(r) - F_{rep}(r) \approx \frac{U_0}{r_0} \frac{mn}{n-m} \left[\left(\frac{r_0}{r}\right)^{m+1} - \left(\frac{r_0}{r}\right)^{n+1} \right] \sim \frac{U_0}{r_0} \frac{mn}{n-m} \left(\frac{r_0}{r}\right)^{m+1} \xrightarrow{r \rightarrow \infty} 0 \quad (20)$$

Consequently, when r is large enough, the attractive forces are effective, moreover, the maximum of the resultant force, F^* , is positive as well:

$$F^* = F(r^*) \approx \frac{U_0}{r_0} \frac{mn}{n+1} \left(\frac{m+1}{n+1}\right)^{\frac{m+1}{n-m}}, \quad r^* = r_0 \left(\frac{n+1}{m+1}\right)^{\frac{1}{n-m}} > r_0 \quad (21)$$

The Lennard-Jones potential is widely used to model adsorption-induced deformation in microporous materials by simulating the interaction between gas molecules and pore walls [34]. It is also applied to study the thermodynamic properties of simple fluids (Lennard-Jones fluids), like compressibility and pressure-volume-temperature relationships, providing an approximation of fluid behavior near ideal gas conditions [35, 36]. Initially developed for noble gases, its application to other systems may introduce inaccuracies, and variations of the potential exist to address these limitations, each producing different macroscopic properties depending on the specific system being studied [37].

3 Results and discussion

In this section, the applicability of the statistical models developed above are tested by numerical calculations based on physical data of atoms and their bonds and demonstrated with a practical example.

3.1 Estimation of electron residence probabilities

3.1.1 First approximation of the ERP based on electronegativity

The dipole moment strongly depend on the electronegativity of the covalent-bonded atoms [38]. Knowing the electronegativities of the two atoms of the dipole, EN_i ($i = 1, 2$), we can obtain a simple (although rough) estimate of the electron residence probabilities (ERP: p_i) using the ratios ϕ_i (Eq. 22):

$$p_i \approx \phi_i = \frac{EN_i}{\sum EN} \quad (22)$$

And DI can also be expressed by ϕ_i :

$$DI = |\mathbf{E}(\delta_i)| = |1 - 2p_i| \approx \frac{\Delta EN}{\sum EN} \quad (23)$$

where ΔEN and $\sum EN$ are the absolute difference and the sum of the EN s of the two atoms, respectively:

$$\Delta EN = |EN_1 - EN_2|, \quad \sum EN = EN_1 + EN_2 \quad (24)$$

Using the Pauling electronegativity scale values [38] and applying Eq. 24, we represented the electronegativities of different atomic pairs in a bonding plot of van Arkel-Ketelaar triangles of (Fig. 3/a). The electron probabilities and the predicted DI (expected charge distribution) values (estimated from Eqs. 22 and 23) are shown in Fig. 3/b. We carried out the analysis for 233 different pairs of atoms, including nonmetallic–nonmetallic (NM–NM: 45), metallic–metallic (M–M: 78) and nonmetallic–metallic (NM–M: 108) pairs [39]. A comparison of the calculated results (Fig. 3/b) with van Arkel-Ketelaar triangles of bonding (Fig. 3/a) indicates that the edges of the triangle are distorted into a symmetric shape bounded by curved arcs, but it retains its domain structure.

3.1.2 Estimation of the ERP based on bond parameters and electronegativities

As Fig. 3/b shows, p_i is the highest for a metal–nonmetal pair, fluorine–cesium (F–Cs), where $p_{F-Cs}=4/4.7=0.8511$ ($\Delta EN=3.3$). However, fluorine and cesium will form an ionic compound, therefore it is assumed that $p_{F-Cs} \approx 1$. Consider another point in the metallic–nonmetallic relationship, the phosphorus–boron (P–B) pair. Of all the examined metallic–non-metallic pairs, this one has the lowest ΔEN (0.1). In this case, $p_{P-B}=2.1/4.1=0.5122$. Again, a larger p_i value would be expected. Consequently, Eq. 22 does not properly describe the relationship between the ERP (p_i) and

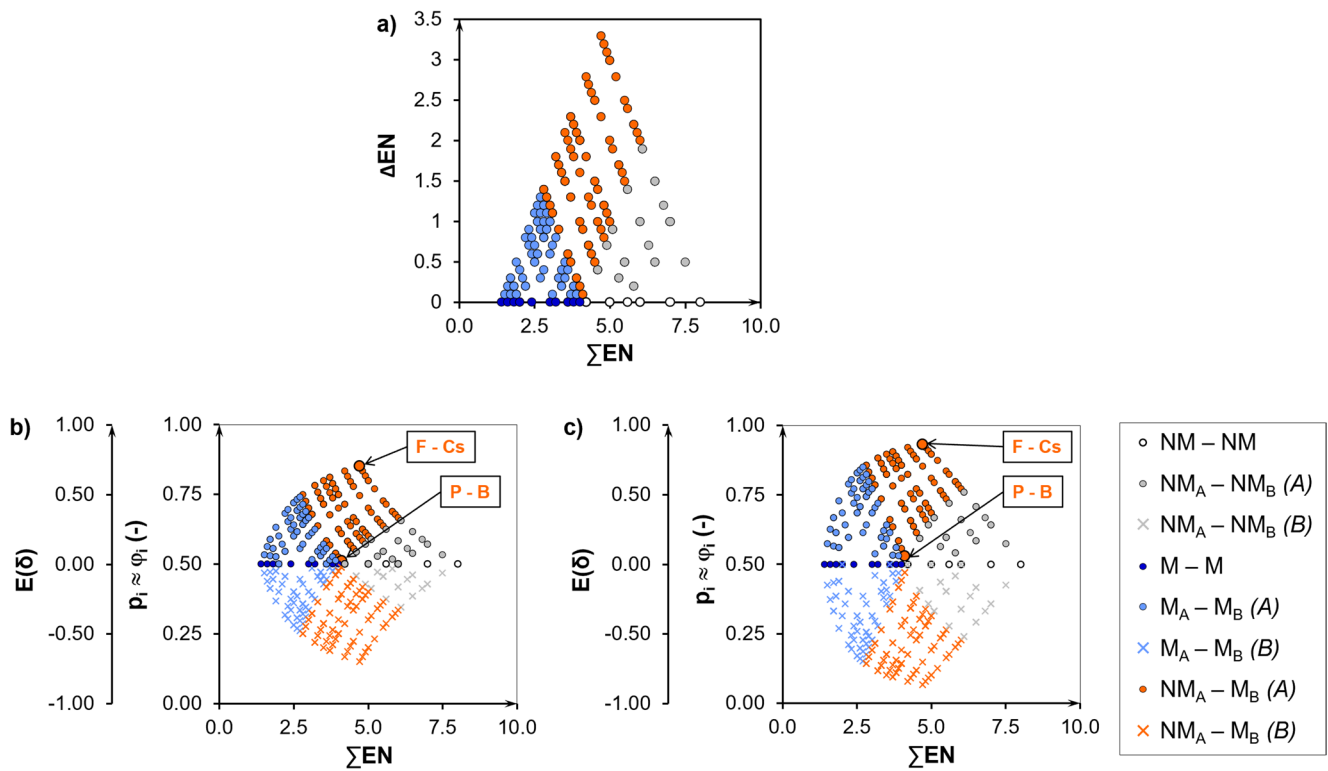


Fig. 3 Trends in electronegativity for different pairs of atoms: **(a)** van Arkel-Ketelaar triangles of bonding, **(b)** estimation of the electron residence probabilities with Eq. 22 **(c)** estimation of the electron residence probabilities with Eq. 26

the electronegativity ratio (ϕ_i). In the literature, we did not find any mathematical model which describes the entire van Arkel-Ketelaar triangles of bonding. Therefore, analysing the relationships between the electron resident probability, p_i , and the electronegativity ratio, ϕ_i , based on the Lennard-Jones potential and Coulomb’s law, and the bonding parameters U_0 and r_0 , we found two formulae suitable for estimating the relationships between them (see in the Supplementary). Accordingly, if we know the bonding parameters of dipole in question Eq. 25 can be applied to estimate the electron resident probability, p_1 :

$$p_1 = \frac{1}{2} \left[1 \pm \sqrt{\frac{1}{3} (4\Omega_0 - 1)} \right], \quad \Omega_0 = \frac{r_0 U_0}{k Q_e^2} \quad (25)$$

where $k=1/(4\pi\epsilon_0)$ is constant, $\epsilon_0=8.8542 \cdot 10^{-12} \text{ c}^2\text{N}^{-1}\text{m}^{-2}$ is the permittivity of vacuum, r_0 is the bond distance determining the global minimum, U_0 is the dissociation energy of the system and $Q_e=-1.61022 \cdot 10^{-19} \text{ C}$ is the electric charge of an electron.

Otherwise, if only the electronegativity values are known for a diatomic system, the ERP (p_i ; $i=1, 2$) can be assessed from ϕ_i using the trend function according to Eq. 26.

$$p_i \approx h(\phi_i) = \frac{1}{2} \left[1 + (2\phi_i - 1) \left(3 - 2|2\phi_i - 1|^{0.35} \right) \right] \quad (26)$$

The related considerations and the derivation of Eqs. 25 and 26 can be found in the Supplementary material. Thus, if only the electronegativity values are known for a diatomic system, the ERP (p_i) can be calculated using Eq. 26. If the bonding parameters are known, the ERP (p_i) can be calculated using Eq. 25. The derivation of Eqs. 25 and 26 can be found in the Supplementary material.

Figure 3/c shows the p_i and $E(\delta_i)$ results calculated with Eq. 26. A comparison of Figs. 3/b and c indicates that the minimum p_{P-B} value increased from 0.5122 to 0.5299 and so did the maximum for p_{F-Cs} from 0.8511 to 0.9328.

3.2 Simplified stochastic model of dipole pairs and secondary bonds

Considering a system of two dipoles with interacting ends (Fig. 4/a) may form a secondary bond when the attractive and repulsive forces balance each other out. The interaction in this state can be characterised with the correlated change of the end-charges and the expected attractive force described by Coulomb’s law based Eq. 7. On the other hand, according to Eq. 12, this interaction can be a distribution transformation of the state probabilities of the ends given for a large distance.

However, it is much simpler to characterise the phenomenon by a concept-based estimation of the states at

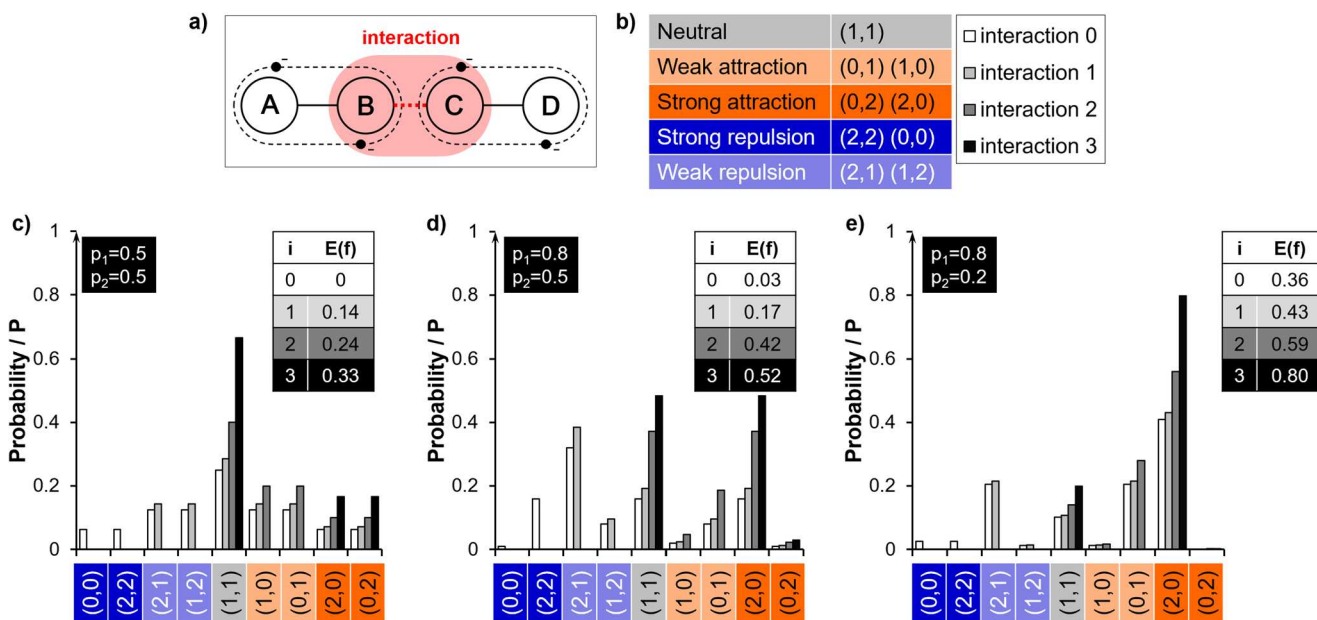


Fig. 4 Electron residence probabilities and interactions for uncorrelated (interaction 0) and correlated (interactions 1, 2, 3) dipoles pairs: (a) two dipole ends as a system, (b) possible states of the two-dipole

system, the residence probabilities of electrons in the case of (c) two apolar instantaneous dipoles (d) a permanent dipole and an apolar dipole (e) two permanent dipoles

equilibrium. Figure 4/b shows the possible states of the two dipole ends as a system (Fig. 4/a) given by electron numbers. Figure 4/c shows the state probabilities of instantaneous dipole pairs ($p_1=p_2=0.5$) as an uninteracted (Interaction_0) independent dipole pair. Due to the axial symmetry of the probabilities, the expected force is zero ($E(f)=0$). The interaction is strongly repulsive in the (0,0) and (2,2) states, strongly attractive in the (0,2) and (2,0) states, and neutral in the (1,1) states. According to Eq. 7, the states (0,1), (1,0), (1,2) and (2,1) can also be considered neutral. But in these cases, a charged end faces a neutral one. Therefore, it can be assumed that a weak repulsive/attractive force (αF_0 ; $0 < \alpha \ll 1$) can arise between them, where α is an arbitrarily small reducing constant. This is positive in the cases of (0,1) and (1,0), where there is a neutral end (with 1 electron) facing an electron-deficient positive end, and negative in the

cases of (1,2) and (2,1), where a negative end (with 2 electrons) is facing a neutral end (with 1 electron). In the following, for illustrative calculations, we use $\alpha=0.1$ as Fig. 5/a shows. Simple model weight distributions can be used to study different types of dipole couplings and interactions. Figure 5/b shows such simple weight distributions, where the weights w_{ij} are 0 or 1. The increase in the number of interactions indicates a trend towards stronger interaction, meaning stronger and stronger attractive effects:

- Interaction_0: distant dipoles, no interaction between them;
- Interaction_1: no strong repulsion, $w_{0,0}=w_{2,2}=0$;
- Interaction_2: no repulsion, $w_{0,0}=w_{2,2}=w_{2,1}=w_{1,2}=0$;
- Interaction_3: strong attraction or neutrality, $w_{0,0}=w_{2,2}=w_{2,1}=w_{1,2}=w_{1,0}=w_{0,1}=0$.

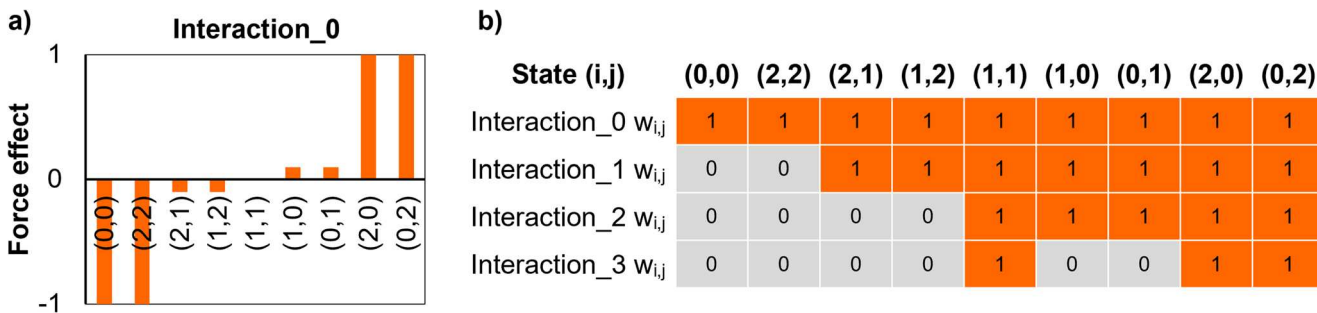


Fig. 5 (a) Possible normalised interactive forces between distant dipole ends as a function of the end states (b) Weight distributions modifying the possible states of a dipole pair

The tables in the Appendix summarizes the algorithmic steps of the method introduced above to support applications. The proposed model sacrifices orbital-specific details but captures bulk electrostatic behaviours. To construct the electron residence probability (ERP) model, several simplifying assumptions are made. These assumptions formalize the physical picture of the covalent bond, enabling the probabilistic treatment of electron locations:

- Two-atom system in a steady state – The system consists of two atoms connected by a single covalent bond, described by a three-dimensional molecular orbital that contains one electron pair. The system is considered stationary at a given (in this case, ambient) temperature, with all parameters remaining constant over time.
 - Electron density as probability measure – The electron residence probability (ERP) within a finite spatial region is obtained by integrating the electron density function over that region.
 - Space partitioning by a separation plane – The system is divided by a separation plane perpendicular to the axis of the two-atom system, defined as the straight line connecting the centers of gravity of the two atoms. This plane divides space into two non-overlapping half-spaces, each representing the vicinity of one atom.
 - Model electrons as independent entities – Two model electrons of identical properties represent the two real electrons. These model electrons move randomly and independently in space, without explicit electron–electron interactions, aside from the inherent property of avoiding occupying the same position.
 - Definition of electron residence probabilities (EPR) - The probability of finding an electron in the vicinity of atom #1 (A1) or atom #2 (A2) is denoted by p_1 and p_2 , respectively, where $p_1 + p_2 = 1$. These probabilities are obtained by integrating the electron density over the respective half-spaces.
- Due to the continuity of the electron density, the probability of an electron lying exactly on the separation plane is zero.
 - Stochastic representation of electron location- Random variables X_{1i} and X_{2i} ($i=1, 2$) indicate the position of the i -th electron relative to atom #1 (A1) or atom #2 (A2). For atom #1, $X_{1i}=1$ if the electron is in its vicinity and $X_{1i}=0$ otherwise. Thus, $P(X_{1i}=1)=p_1$ and $P(X_{1i}=0)=p_2$. The variables X_{1i} and X_{1j} are independent and identically distributed according to a Bernoulli distribution with parameter p_1 . Their sum, $X_1=X_{11}+X_{12}$, follows a binomial distribution $Bin(2, p_1)$. Similarly, $X_2=X_{21}+X_{22}$, follows a binomial distribution $Bin(2, p_2)$.
 - Nature of interaction – Secondary bonds are treated as special interactions between two dipoles formed by pairs of atoms connected by single covalent bonds.
 - Dipole alignment – The axes of the interacting dipoles, defined by the line connecting the centers of gravity of the bonded atoms, are assumed to coincide, while dynamic effects are neglected.
 - Interaction site – The interaction arises specifically between the two facing ends of the aligned dipoles.
 - Steady-state condition – The dipoles are considered to be in steady state under the given temperature conditions.
 - Charge fluctuations at dipole ends – Each dipole end is assumed to carry a randomly varying electric charge, determined by the corresponding electron residence probability (ERP) as previously defined.
 - Force estimation – The instantaneous force between the randomly charged dipole ends is approximated by Coulomb's law at any finite separation distance.
 - Potential energy approximation – The potential energy of the dipole–dipole system is approximated using the Lennard–Jones potential function.

Figure 6 shows a schematic representation of primary (a) and secondary bonding (b). The calculation steps, equations,

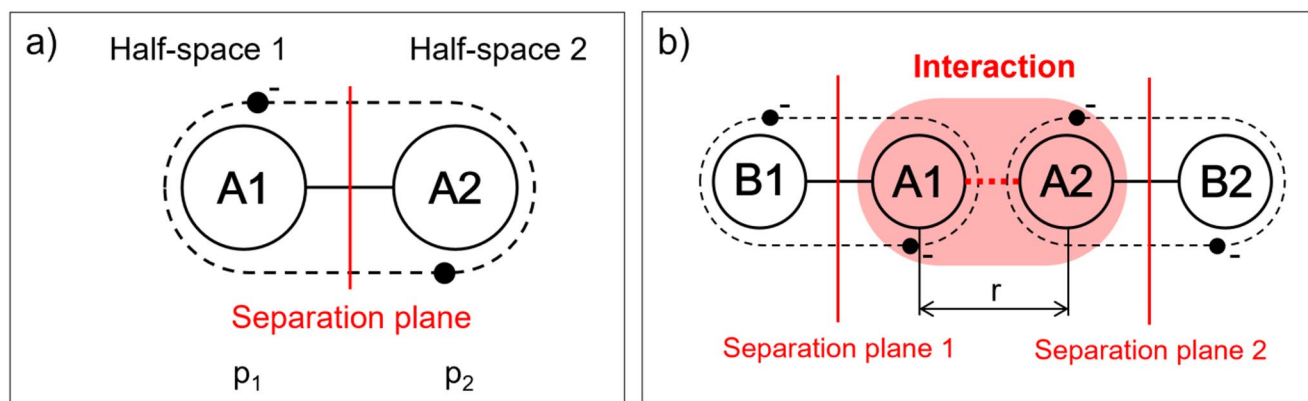


Fig. 6 Schematic representation of primary (a) and secondary bonding (b) within the proposed theoretical framework

and input parameters are presented in the Appendix (Tables 4 and 5).

We compared the fundamental properties of the proposed ERP method with well-established FF methods, as presented in Table 1. Density functional theory is an electronic structure method that approximates electron correlation through density functionals and generally has good accuracy over geometries and energetics at a moderate cost, making it widely applicable to medium-sized systems. The Hartree-Fock method is a mean-field wavefunction approximation that neglects dynamical correlation, which often underestimates and overestimates dispersion, and is therefore commonly used as a reference or starting point for correlated methods. The molecular mechanics force fields are empirical methods that use bond terms, Lennard-Jones potentials, and fixed partial charges. Their main advantage is that

they are widely parameterizable and transferable to molecules and liquids, and have a relatively low computational cost for fixed charges. However, much more computationally demanding extensions are required to model polarized systems or chemical bond formation or breaking. Our method provides a compact, physics-based mapping from electronegativity to electron residence probabilities, resulting in closed-form dipole and modified Lennard-Jones potentials, providing a meaningful, parameter-poor description of chemical bonds. Because it uses simple algebraic expressions instead of solving the electron problem, ERP is faster than DFT or HF methods and, although based on electron behavior rather than purely empirical MM force fields, is simple enough to be embedded in multiscale and kinetic models or high-throughput filtering.

Table 1 Comparison of the fundamental properties of the proposed method with other commonly used force field (FF) methods

	Density Functional Theory (DFT) method	Hartree-Fock (HF) method	Molecular mechanics force fields	Proposed method
Foundational approach	Focuses on the electron density as the primary variable	Uses wavefunctions as the primary variable, approximates the many-electron problem by mean-field approximation	Classical molecular mechanics: empirical functional form with explicit bonded terms (bond, angle, dihedral) + pairwise non-bonded interactions)	Using functional forms such as Coulomb's law and the Lennard-Jones potential
Treatment of electron correlation	Incorporates electron correlation effects through exchange-correlation functionals	Does not explicitly account for electron correlation	Fixed-charge FFs do not treat electron correlation or induction, polarizable FF extensions exist	Electron correlation is characterised with the correlated change of the end-charges
Methodology	Ab initio	Ab initio	Empirical (classical) molecular mechanics force fields	Do not directly account for the quantum mechanical nature of electrons
Computational cost	Simplifies the many-body problem by focusing on electron density, therefore more efficient	Less expensive than DFT but may be less accurate	Fixed-charge FFs: low, polarizable or reactive variants: significantly more expensive	Low
Accuracy	Depends on the choice of functional	Reasonable approximation for systems where electron correlation is not critical	Reliable, extensively benchmarked, fixed-charge FFs miss many-body induction; polarizable FFs improve accuracy	Reasonable approximation for bonding force of primary and secondary bonds in diatomic systems or dipoles
Purpose	Calculating molecular properties (energies, geometries, and electronic structures)	Starting point for more advanced methods	General molecular dynamics, fixed-charge FFs: efficient large-scale MD; polarizable/reactive variants: induction or bond reactivity	Distance-dependent description of the force field between two atoms/dipoles

Table 2 Product of the instantaneous dipole charges in the ideal $(\delta_{11}, \delta_{12})$ and the possible (δ_1, δ_2) cases depending on the numbers of electrons on the facing ends

(X_1, X_2)	(0,0)	(2,2)	(2,1)	(1,2)	(1,1)	(1,0)	(0,1)	(2,0)	(0,2)
$(\delta_{11}, \delta_{12})$	(1,1)	(-1,-1)	(-1,0)	(0,-1)	(0,0)	(0,1)	(1,0)	(-1,1)	(1,-1)
$-\delta_{11}\delta_{12}$	-1	-1	0	0	0	0	0	1	1
(δ_1, δ_2)	(1,1)	(-1,-1)	(-1,-0.1)	(-0.1,-1)	(0,0)	(0.1,1)	(1,0.1)	(-1,1)	(1,-1)
$-\delta_1\delta_2$	-1	-1	-0.1	-0.1	0	0.1	0.1	1	1

The proposed electron-residence-probability model sits between simple empirical force fields and complicated quantum chemistry, as it estimates, for each bonded pair, how likely the shared electron is to reside nearer one atom or the other, and converts that probability into a distance-dependent dipole and a compact bonding potential. In practice ERP gives a simple analytic rule that captures the essential physics of pairwise charge sharing and hydrogen bonding while remaining cheap to evaluate, thus it is comparable in cost to classical force-field terms. By contrast, ab-initio methods such as density functional theory (DFT) or high-level wavefunction approaches solve the electronic problem for the whole molecule. They capture many-electron effects, polarization across a molecule, charge transfer, and accurate reaction energetics, but at significantly higher computational cost, whereas high-accuracy methods are feasible only for very small systems and scale steeply with size. However, ERP is fundamentally a two-body model and does not self-consistently account for many-body polarization or subtle electronic delocalization; DFT and post-HF methods do, albeit at much greater cost. In practical workflow, both methods can be used simultaneously, ab-initio calculations may be used on small representative fragments to obtain dissociation energies and distances (U_0, r_0), and then ERP can be used for large-scale molecular dynamics or multiscale simulations. When needed, residual errors can be addressed by machine-learning corrections as well.

3.3 Modelling the H-bond with the proposed stochastic model

As a practical application example, let us consider water molecules, where two identical dipoles (O-H...O-H) interact, and the hydrogen atom forms a sort of bridge between the two oxygen atoms. The calculations follow the algorithmic steps summarized in the Appendix.

3.3.1 Parameters of the dipoles

The electronegativities for the H and the O atoms are 2.1 and 3.5, the corresponding electronegativity ratios $\phi_1 = 0.375$ and $\phi_2 = 0.625$, respectively. Bond length is $r_0 =$

0.197 nm and the dissociation energy is $U_0 = 21$ kJ/mol [40, 41]. For both dipoles, the electron residence probabilities estimated with Eq. 25 came to about $p_1 = 0.2837$ at the H-end and $p_2 = 0.7163$ at the O-end. They differ significantly from the electronegativity ratios.

3.3.2 Parameters of the secondary bond

Corresponding to the assumption in Chap. 3.2 concerning the possible (normalized) force effect between the dipoles depicted in Fig. 5a; Table 2 shows the product of the possible charges at different states of the facing dipole ends.

3.3.3 Calculation of the mean product of charges for interactions I0,...,I3

Based on the bond energy and distance data and using the transformed joint probabilities by Eq. 12 and the transformation weights in Fig. 5/b, we first calculated the mean product of the possible charges (Table 2), $G(r) = E(g(r, t)) = -E(\delta_1\delta_2)$ (Table 3) using Eq. 7. The other quantities in Table 3 including the correlation coefficient $R(\delta_1, \delta_2)$ are calculated with Eqs. 7–9.

In the case of distant dipoles, their distance should be larger than the separation distance (r_{sep}), where the interaction between the dipoles can be neglected (Interaction_0). Thus, for $r_{1_0} \geq r_{sep}$, $G_\infty = \lim_{r \rightarrow \infty} G(r) \approx G(r_{1_0}) = 0.1872$ (Table 3) is approximately constant while, based on Coulomb's law and the Lennard-Jones potential (Eqs. 7 and 21), the $G(r) - G_\infty$ difference depends on the distance $r_0 \leq r \leq r_{1_0}$ where $G(r_0) = G(r_{1_3}) = 0.6203$ regarding Interaction_3 for the H-bond (Table 3). As for r_{sep} , it is

Table 3 Parameters of the joint and marginal distributions, the estimated mean normalised force and the correlation parameters at different interactions for the H-bond between water molecules

O-H...O-H	Interaction_0	Interaction_1	Interaction_2	Interaction_3
$G(r) = -E(\delta_1\delta_2)$	0.1872	0.2941	0.4346	0.6203
r/r_0	2.00	1.32	1.12	1.00
$E(f)$	0.0468	0.1680	0.3475	0.6203
$E(\delta_1)E(\delta_2)$	0.1872	0.2224	0.2281	0.3487
$D(\delta_1)D(\delta_2)$	0.4064	0.3346	0.2808	0.2716
$C(\delta_1, \delta_2)$	0.0000	0.0716	0.2065	0.2716
$R(\delta_1, \delta_2)$	0.0000	0.2141	0.7354	1.0000

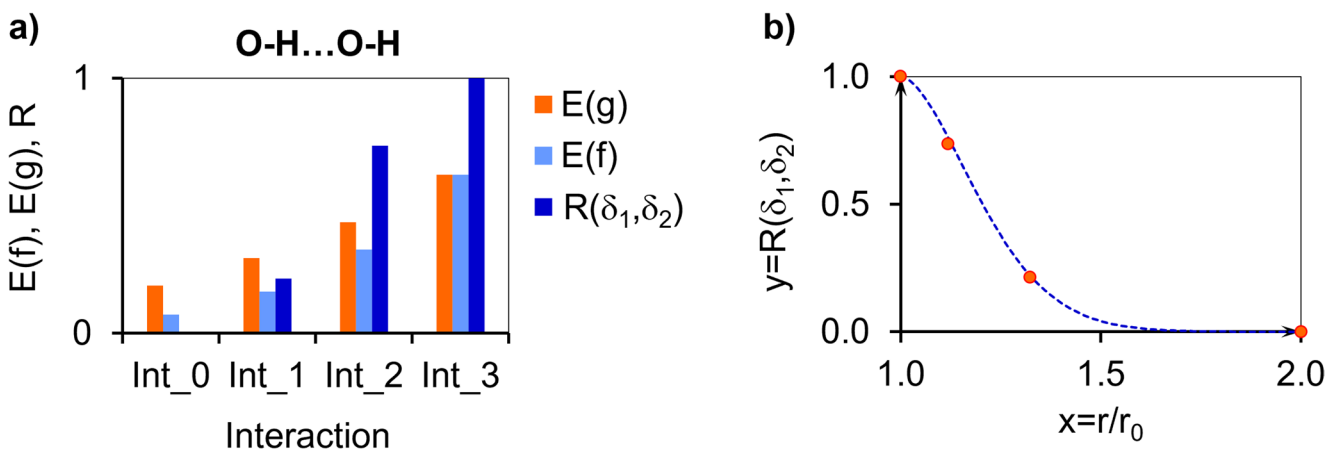


Fig. 7 Mean normalised force, $E(f)$, and the charge interaction parameters $E(g)$ and the space correlation coefficient $R(\delta_1, \delta_2)$ for the H-bond between water molecules at different interactions (a), and as a function of distance (r/r_0) (b)

not smaller than 3 nm [42] that is $r_{sep} \geq 1.52r_0$ meaning that $r_{I_0} = 2r_0$ may be reasonable (Table 3). According to Eq. 7, the exponent should be larger than 1 and considering Eq. 21, we chose $m - 1$, where m is the exponent of the Lennard-Jones potential for the attractive force, and obtained the following formula, where r_0 is bond distance and $G_0 = G(r_0)$:

$$G(r) = E(g(r, t)) = G_\infty + (G_0 - G_\infty) \left[\frac{r_0}{r} \right]^{m-1} \xrightarrow{r \rightarrow \infty} G_\infty \quad (27)$$

We followed the practice that for the secondary bond, the same Lennard-Jones exponents ($m=6$ and $n=12$) can be applied as for the covalent bond. Hence, the rearrangement of Eq. 27 provided the proper distances r_{I_k} related to Interaction $_k$ ($k=0, 1, 2, 3$) that belong to the calculated G_k values (Table 2; Fig. 6/a):

$$G_k = G(r_{I_k}) = G_\infty + (G_0 - G_\infty) \left[\frac{r_0}{r_{I_k}} \right]^{m-1} \quad (28)$$

$$\Rightarrow \frac{r_{I_k}}{r_0} = \left[\frac{G_0 - G_\infty}{G_k - G_\infty} \right]^{\frac{1}{m-1}}$$

In this approach, Interaction₃ represents the behaviour of the H-bond at the H-bond length (r_0), where $G_0 = 0.6203$ (Table 3; Fig. 7/a). $G_0 = 0.6203$ means that it is 62% of the possible maximum. This can be a fourth interaction type (Interaction₄) where only the states (2,0) and (0,2) are realized (Fig. 5/b). Consequently, $\delta_2 = -\delta_1$ and their absolute values equal to 1. Therefore $E(\delta_1, \delta_2) = \delta_1 \delta_2 = -1$, this indicates a deterministic state corresponding to a virtual ionic bond. Using Eq. 28 and $G_i = 1$, the normalised length of the ionic bond is $r_{0i}/r_0 = 0.882$ (Fig. 8/a).

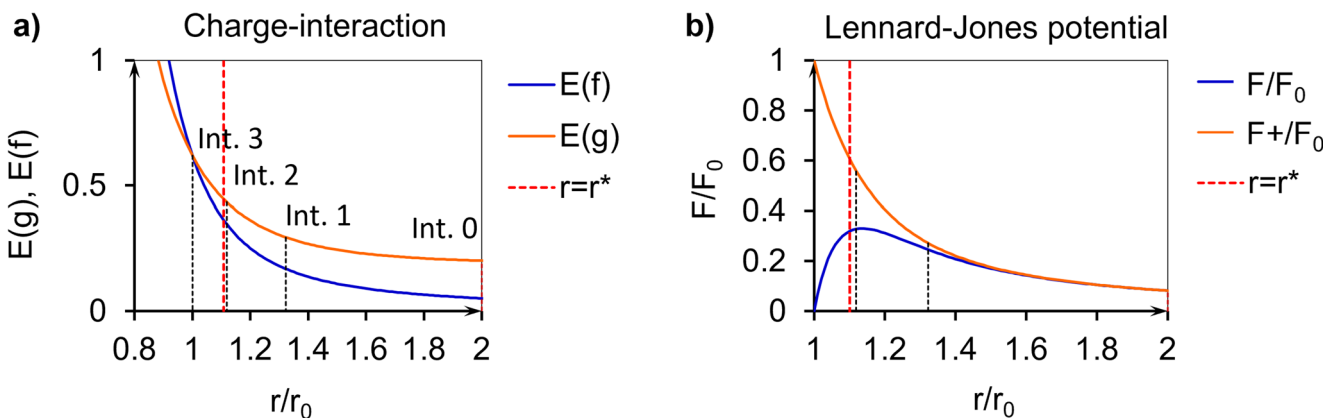


Fig. 8 Mean normalised force, $E(f)$, and interaction parameters $E(g)$ and $R(\delta_1, \delta_2)$ for the H-bond between water molecules as a function of the distance (r/r_0) (a) and normalised force, F/F_0 in the case of different interactions (b)

3.3.4 Calculation of the characteristic functions for the secondary bond

Using Eq. 7 and multiplying Eq. 27 by $(r_0/r)^2$, we obtained the normalised (attractive) interaction force, $\mathbf{E}(f)$ (Table 3; Fig. 8/a):

$$\begin{aligned} \mathbf{E}(f(r, t)) &= \mathbf{E}(g(r, t)) \left[\frac{r_0}{r} \right]^2 \\ &= G_\infty \left[\frac{r_0}{r} \right]^2 + (G_0 - G_\infty) \left[\frac{r_0}{r} \right]^{m+1} \xrightarrow{r \rightarrow \infty} 0 \end{aligned} \quad (29)$$

By calculating the expected values, $\mathbf{E}(\delta_i)$, and the standard deviations, $\mathbf{D}(\delta_i)$, of the transformed marginal distributions according to Eq. 29, we were able to compute the interaction covariance, $\text{Cov}(\delta_1, \delta_2)$, and the correlation coefficient, $R(\delta_1, \delta_2)$ using Eqs. 7 and 9 (Table 2; Fig. 7/a).

As expected, as the strength of the interaction increases, both the mean bonding force ($\mathbf{E}(f)$) and the space correlation coefficient ($R(\delta_1, \delta_2)$) significantly increases (Fig. 7/b), and in Interaction 3, $\mathbf{E}(f)$ reached the 62% of the maximum ideal bonding force (Table 3). At this bonding state ($r=r_0$), the correlation coefficient reached the maximum, which is 1. On the other hand, the interaction correlation coefficient decreased with increasing distance (r). This relationship, which can be considered the reliability of the bonding, could be well-described with a general exponential formula like that of the complementary Weibull's distribution (Eq. 30) (Fig. 7/b):

$$R(r) = \exp \left[- \left(\frac{r - a}{b} \right)^c \right] \quad (30)$$

where the shift was $a=1$, and from the fitting, we obtained $b=0.2532$ and $c=1.70$. Figure 7/b shows that the correlation coefficient drops with increasing distance, then decreases slowly, corresponding to the behavior of the secondary bonds. Consequently, we may state that the increasing strength of the interaction can be characterised by an increasing correlation between the charges of the dipole ends as well, confirming the applicability of the stochastic H-bonding models developed.

We compared our findings with the results of Kumar et al. [20], who used Bader's Quantum Theory of Atoms in Molecules (QTAIM) to model the hydrogen bond in a water dimer. They showed that the electron density (ED) field had a local minimum between the two water molecules, which had been closer to the H-atom. They also showed that ED was increased by decreasing the distance from the weak van der Waals interaction to the moderately

strong H-bond interaction. This observation is consistent with our simple model, in which the behaviour was described as an interaction between independent dipoles at large distances, and the interaction became increasingly correlated, i.e., stronger as the distance decreased.

Because of the two-term formula of the attractive force in Eq. 29, creating a suitable potential function for the H-bond requires a modification of the Lennard-Jones formula by Eq. 20. At the bond length both the attractive and the repulsive forces must be equal to 1. Therefore, we normalised Eq. 29 by G_0 to obtain the attractive term (Eq. 31) and we used Eq. 20 to obtain the repulsive term (Eq. 32):

$$\mathbf{E}(f_H^+(r, t)) = \frac{\mathbf{E}(f(r, t))}{G_0} = \frac{G_\infty}{G_0} \left[\frac{r_0}{r} \right]^2 + \left(1 - \frac{G_\infty}{G_0} \right) \left[\frac{r_0}{r} \right]^{m+1} \quad (31)$$

$$\mathbf{E}(f_H^-(r, t)) = \left[\frac{r_0}{r} \right]^{n+1} \quad (32)$$

Hence, on the analogy of the Lennard-Jones function (Eq. 20), we constructed the following H-bonding force function, which gives 0 at $r=r_0$, as required:

$$\begin{aligned} F_H(r) &= \frac{U_0}{r_0} \frac{mn}{n-m} \left[\mathbf{E}(f_H^+(r, t)) - \mathbf{E}(f_H^-(r, t)) \right] \\ &= \frac{U_0}{r_0} \frac{mn}{n-m} \left[\frac{G_\infty}{G_0} \left[\frac{r_0}{r} \right]^2 + \left(1 - \frac{G_\infty}{G_0} \right) \left[\frac{r_0}{r} \right]^{m+1} - \left[\frac{r_0}{r} \right]^{n+1} \right] \end{aligned} \quad (33)$$

Integrating Eq. 28 provided the H-bonding potential function, which was completed with an additive constant in order to meet the condition $U_H(r_0)=-U_0$:

$$U_H(r) = U_0 \frac{mn}{n-m} \cdot \left[-\frac{G_\infty}{G_0} \frac{r_0}{r} - \left(1 - \frac{G_\infty}{G_0} \right) \frac{1}{m} \left[\frac{r_0}{r} \right]^m + C_{m,n} + \frac{1}{n} \left[\frac{r_0}{r} \right]^n \right] \quad (34)$$

$$U_H(r_0) = -U_0 \Rightarrow C_{m,n} = \frac{m-1}{m} \frac{G_\infty}{G_0} \quad (35)$$

The H-bonding potential function according to Eq. 35 meets every condition as does the Lennard-Jones function by Eq. 20. At the same time, the former describes long-range interaction as well (Fig. 8/b). Thus, we obtain a modified Lennard-Jones potential, in which we take into account, by Coulomb's law, that if there is a very large distance between the two dipoles, and they are already independent of each other, there is still some connection between them. This allows us to take into account the characteristic of the secondary bond that some kind of connection between the connected dipoles can be interpreted even at infinite distances.

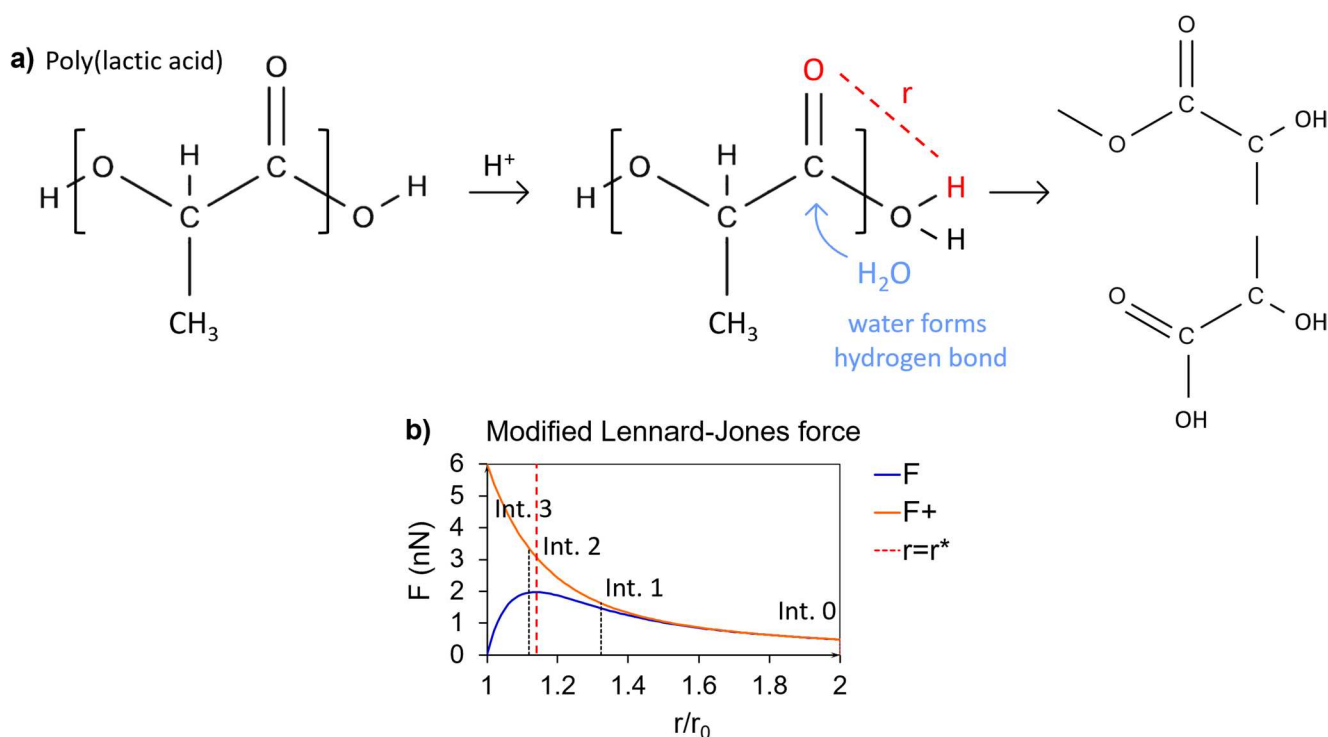


Fig. 9 Hydrolysis of PLA (based on [43]) (a) and the distance-dependent force between the highlighted O and H atoms (b)

3.4 Potential applications

In the following, we describe a potential practical application of the findings for polymer materials. When polylactic acid (PLA) absorbs moisture, water molecules primarily interact with the ester functional groups in the polymer chain. Water molecules can form hydrogen bonds with the carbonyl oxygen (C=O) in the ester group of PLA. Over time, hydrolysis may occur meaning that the water molecules break down the ester bonds. This leads to the degradation of PLA, where water attacks the ester bond, cleaving it and forming carboxylic acid (-COOH) and alcohol (-OH) groups in the polymer chain (Fig. 9/a). Hydrolysis primarily starts near the chain ends where -OH and -COOH groups are present. The closer the carboxyl end groups are to the ester bonds, the more efficient the catalysis becomes. Shorter distances allow the -COOH groups to interact more readily with the ester bonds, promoting the hydrolysis reaction. Using the model presented in this paper, the force and the interaction parameters can be given as a function of the distance between the highlighted O and H atoms (Fig. 9/b). The figure shows the distance-dependent force between the two atoms at different interactions. These output data can help to more accurately model the accelerated hydrolysis process. The case of PLA hydrolysis demonstrates atomistic modeling of water-polymer interactions. The modelling approach could be translated into predictive tools for degradation. Atomistic modeling of hydrolysis provides

the fundamental interaction parameters—such as distance-dependent forces between water molecules and ester groups—that provide the basis for the bond cleavage of biodegradable polymers. If incorporated into atomic-level simulations, the modelling framework can help to quantify how water molecules bind to carbonyl oxygen via hydrogen bonds, how end groups catalyze cleavage, and how the local environment influences activation energies. This would provide rate constants and catalytic factors that could be directly incorporated into continuous reaction-diffusion models. Future work should focus on predictive frameworks to go beyond empirical fitting and instead use chemistry-specific input data, making lifetime predictions more transferable across different compositions and environmental conditions.

4 Conclusion

We introduced a unified, stochastic framework to describe both primary (covalent) and secondary bonds in polymeric materials using nothing more than elementary probability and classical force laws. By defining an electron residence probability (ERP) for each interacting pair, and combining Coulomb's law with a modified Lennard-Jones potential, we derived closed-form expressions for both bond forces and interaction energies

as explicit functions of interatomic distance. The space correlation function can characterize the strength of the interaction between two dipoles. Our analytic ERP formulas recovered established behavior at the extremes of the van Arkel–Ketelaar bonding triangle—ionic, covalent, and metallic regimes—and interpolated smoothly across the full domain of electronegativity differences. The model’s versatility was demonstrated through a case study of O–H interactions during polylactic acid (PLA) hydrolysis: predicted force curves and energy profiles agreed closely with high-fidelity force-field simulations while requiring only a fraction of the computational

effort. Because the entire framework rests on transparent probabilistic concepts and readily evaluable algebraic expressions, it can be straightforwardly embedded into kinetic models, continuum-scale simulations, or multi-scale coupling schemes. Our approach thus bridges the gap between detailed quantum-mechanical treatments and oversimplified classical force-field potentials, offering materials scientists and engineers a principled yet accessible tool for rapid, physics-based modelling of bond formation, breaking, and rearrangement in complex material systems.

Appendix

Table 4 Determination of the electron residence probability (ERN) in a dipole of given single covalent-bonded atom-pair A1-A2

Task	Operation/Data	Remark
1. Parameters of the covalent bond are available		
1.1. Input data	bond parameters r_0 and U_0	from database
1.2. Calculation of ERNs	$p_1 = \frac{1}{2} \left[1 + \sqrt{\frac{1}{3} \left(4 \frac{r_0 U_0}{k Q_e^2} - 1 \right)} \right], \quad p_1 = 1 - p_2$	Equation 25 constants: k and Q_e
2. Parameters of the covalent bond are not available		
2.1. Input data	electronegativity EN_1 and EN_2	from database
2.2. EN ratios	$\phi_1 = EN_1 / (EN_1 + EN_2), \phi_2 = 1 - \phi_1$	Equation 22
2.3. Estimation of ERNs	$p_1 \approx h(\phi_1)$ $= \frac{1}{2} \left[1 + (2\phi_1 - 1) (3 - 2 2\phi_1 - 1 ^{0.35}) \right]$ $p_2 \approx h(\phi_2) = 1 - p_1$	Equation 26

Table 5 Determination of the parameters and function properties of a secondary bond created by two given dipoles B1-A1...A2-B2 (The facing dipole-atoms are A1 and A2.) (In the example: O-H...O-H)

Task	Operation/Data	Remark	
1.	Parameters of the dipoles B1-A1 and A2-B2		
1.1.	Determination of ERNs	$p_1 = p_{A1}(B1-A1), p_2 = p_{A2}(A2-B2)$	Equation 25 or 26
1.2.	Calc. of dipole E	$\mathbf{E}(\delta_i) = \mathbf{E}(1 - X_i) = 1 - 2p_i$	Equations 3 and 4
1.3.	Calc. of dipole SD	$\mathbf{D}(\delta_i) = \mathbf{D}(X_i) = \sqrt{2p_i(1 - p_i)}$	SD of Bin(2, p_i)
2.	Parameters of the secondary bond		
2.1.	Available input data	secondary bond parameters r_0 and U_0	from database or literature/measured
	Roughly assessed input data	data pairs based on intervals $[r_{01}, r_{02}]$ and $[U_{01}, U_{02}]$: (r_{01}, U_{02}) and/or (r_{02}, U_{01})	found in database or literature
2.2.	Determination of the LJ-exponents	$m=6, n=12$	usual data in literature
3.	Calculation of the mean product of charges for Interactions I0,...,I3		
3.1.	Calc. of probs. $p_{i,j}$	$p_{i,j} = \mathbf{P}(X_1 = i, X_2 = j) = q_{2,i}q_{2,j}$	Equation 10
3.2.	Calc. of weights $W_{i,j}$	$W_{i,j} = \frac{w_{i,j}}{\sum_{i,j=0}^2 w_{i,j} p_{i,j}}$	Equation 15; $w_{i,j}$: Fig. 5b; Table 2
3.3.	Calc. of probs. $\hat{p}_{i,j}$	$\hat{p}_{i,j} = W_{i,j} p_{i,j}$	Equation 12
3.4.	Calc. of $G(r_{I_k})$	$G_k = G(r_{I_k}) = -\mathbf{E}(\delta_1 \delta_2)(r_{I_k}) = -\sum_{(i,j)} \delta_i \delta_j \hat{p}_{i,j}$ r_{I_k} ($k=0, 1, 2, 3$) is the distance of dipoles for Interaction I _k	Tables 2 and 3
3.5.	Determination of parameters of G(r) for bond O-H...O-H	$G_0 = G(r_{I_3})$	Equation 27
3.6.	Calc. of r_{I_k}/r_0 for I0,..,I3	$G_\infty \approx G(r_{I_0})$ $\frac{r_{I_k}}{r_0} = \left[\frac{G_0 - G_\infty}{G_k - G_\infty} \right]^{\frac{1}{m-1}}$	Equation 28
4.	Calculation of the characteristic functions for the secondary bond		
4.1.	Calc. of the mean normalized force	$\mathbf{E}(f(r, t)) = G_\infty \left[\frac{r_0}{r} \right]^2 + (G_0 - G_\infty) \left[\frac{r_0}{r} \right]^{m+1}$	Equation 29
4.2.	Calc. of covariance	$Cov(\delta_1, \delta_2) = \mathbf{E}[\delta_1 \delta_2] - \mathbf{E}(\delta_1) \mathbf{E}(\delta_2)$	Equation 8
4.3.	Calc. of correlation	$R(r) = R(\delta_1, \delta_2)(r) = \frac{Cov(\delta_1, \delta_2)}{\mathbf{D}(\delta_1) \mathbf{D}(\delta_2)} = \exp \left[- \left(\frac{\frac{r}{r_0} - a}{b} \right)^c \right]$	Equations 9 and 30, pars. $a, b,$ and c are fitted
4.4.	Calc. of the H-bond force function	$F_H(r) = \frac{U_0}{r_0} \frac{mn}{n-m} \left[\frac{G_\infty}{G_0} \left[\frac{r_0}{r} \right]^2 + \left(1 - \frac{G_\infty}{G_0} \right) \left[\frac{r_0}{r} \right]^{m+1} - \left[\frac{r_0}{r} \right]^{n+1} \right]$	Equation 33
4.5.	Calc. of the H-bond potential function	$U_H(r) = U_0 \frac{mn}{n-m} \left[-\frac{G_\infty}{G_0} \frac{r_0}{r} - \left(1 - \frac{G_\infty}{G_0} \right) \frac{1}{m} \left[\frac{r_0}{r} \right]^m \right]$ $S + C_{m,n} + \frac{1}{n} \left[\frac{r_0}{r} \right]^n, \quad C_{m,n} = \frac{m-1}{m} \frac{G_\infty}{G_0}$	Equation 34

(LJ – Lennard-Jones, Calc. – Calculation, probs. – probabilities, Bin – Binomial distribution)

Acknowledgements Project no. TKP-6-6/PALY-2021 has been implemented with the support provided by the Ministry of Culture and Innovation of Hungary from the National Research, Development and Innovation Fund, financed under the TKP2021-NVA funding scheme. Ábris Dávid Virág is thankful for the support of the EKÖP-25-4-II-BME-212 University Research Fellowship Programme of the Ministry for Culture and Innovation from the source of the National Research, Development and Innovation Fund. Csenge Tóth is thankful for the support of the EKÖP-25-4-II-BME-214 University Research Fellowship Programme of the Ministry for Culture and Innovation from the source of the National Research, Development, and Innovation Fund.

Author contributions László Mihály Vas: Conceptualization, Methodology, Formal analysis, Writing – Original Draft.

Csenge Tóth: Conceptualization, Visualization, Writing – Original Draft.

Roland Petrény: Writing – Original Draft.

Ábris Dávid Virág: Conceptualization, Writing – Review & Editing, Supervision.

Funding Open access funding provided by Budapest University of Technology and Economics.

Data availability The data used for the calculations are available in the referenced literature.

Declarations

Conflict of interest The author has no relevant financial or non-financial interests to disclose.

Open Access This article is licensed under a Creative Commons Attribution 4.0 International License, which permits use, sharing, adaptation, distribution and reproduction in any medium or format, as long as you give appropriate credit to the original author(s) and the source, provide a link to the Creative Commons licence, and indicate if changes were made. The images or other third party material in this article are included in the article's Creative Commons licence, unless indicated otherwise in a credit line to the material. If material is not included in the article's Creative Commons licence and your intended use is not permitted by statutory regulation or exceeds the permitted use, you will need to obtain permission directly from the copyright holder. To view a copy of this licence, visit <http://creativecommons.org/licenses/by/4.0/>.

References

1. L. Pauling, The nature of the chemical bond. Application of results obtained from the quantum mechanics and from a theory of paramagnetic susceptibility to the structure of molecules. *J. Am. Chem. Soc.* **53**, 1367–1400 (1931). <https://doi.org/10.1021/ja01355a027>
2. D.S. Levine, M. Head-Gordon, Clarifying the quantum mechanical origin of the covalent chemical bond. *Nat. Commun.* **11**, 4893 (2020). <https://doi.org/10.1038/s41467-020-18670-8>
3. J. Barrett, Structure, Bonding, *R. Soc. Chem.* (2001). <https://books.google.hu/books?id=-zIM6J1gEJkC>
4. G. Bodor, *Structural investigation of polymers.* (Ellis Horwood, 1991). <https://books.google.hu/books?id=QOOFAAAAIAAJ>
5. G.N. Lewis, Valence and the Structure of Atoms and Molecules, Chemical Catalog Company, Incorporated, (1923). <https://books.google.hu/books?id=BTWJAQAIAAJ>
6. W. Wu, P. Su, S. Shaik, P.C. Hiberty, Classical valence bond approach by modern methods. *Chem. Rev.* **111**, 7557–7593 (2011). <https://doi.org/10.1021/cr100228r>
7. C.J. Ballhausen, H.B. Gray, M.O. Theory, Benjamin, (1962). <https://books.google.hu/books?id=6wPiwAEACAAJ>
8. G.H. Wagnière, *Introduction To Elementary Molecular Orbital Theory and To Semiempirical Methods* (Springer-, 1976). <https://books.google.hu/books?id=GATwAAAAMAAJ>
9. L. Salem, The Molecular Orbital Theory of Conjugated Systems, W.A. Benjamin, (1966). <https://books.google.hu/books?id=eEdRAAAAMAAJ>
10. L.C. Allen, J.F. Capitani, G.A. Kolks, G.D. Sproul, Van Arkel—ketelaar triangles. *J. Mol. Struct.* **300**, 647–655 (1993). [https://doi.org/10.1016/0022-2860\(93\)87053-C](https://doi.org/10.1016/0022-2860(93)87053-C)
11. W.B. Jensen, The Historical Development of the van Arkel Bond-Type Diagram *, in: n.d. <https://api.semanticscholar.org/CorpusID:202708892>
12. G. Sproul, Electronegativity and bond type. 3. Origins of bond type. *J. Phys. Chem.* **98**, 13221–13224 (1994). <https://doi.org/10.1021/j100101a023>
13. M. Radaoui, A. Ben Fredj, S. Romdhane, D.A.M. Egbe, H. Bouchriha, Annealing temperature dependence of the performance of bulk heterojunction polymer: fullerene solar cells under short and open circuit conditions. *Synth. Met.* **271**, 116611 (2021). <https://doi.org/10.1016/j.synthmet.2020.116611>
14. M. Radaoui, O. Taboubi, A. Ben Fredj, S. Romdhane, D.A.M. Egbe, H. Bouchriha, Blend ratio and applied voltage effects on the charge recombination in bulk heterojunction polymer solar cells based on anthracene-containing poly(arylene-ethynylene)-alt-poly(arylene-vinylene) studied using magnetoconductance. *J. Phys. Chem. Solids* **156**, 110190 (2021). <https://doi.org/10.1016/j.jpcs.2021.110190>
15. D.J. Griffiths, D.F. Schroeter, *Introduction To Quantum Mechanics*, 3rd edn. (Cambridge University Press, Cambridge, 2018). <https://doi.org/10.1017/9781316995433>
16. N. Bohr, L. Rosenfeld, U. Hoyer, J.R. Nielsen, K. Stolzenburg, E. Rüdinger, R. Peierls, J. Kalkcar, D. Favrholt, F. ?Serud, Collected Works: Foundations of Quantum Physics, I-II: (1926–1958). Vol. 6–7, North-Holland, (1972). <https://books.google.hu/books?id=-3OFwQEACAAJ>
17. K. Burke, Perspective on density functional theory. *J. Chem. Phys.* **136**, 150901 (2012). <https://doi.org/10.1063/1.4704546>
18. D.J. Thouless, Stability conditions and nuclear rotations in the Hartree-Fock theory. *Nucl. Phys.* **21**, 225–232 (1960). [https://doi.org/10.1016/0029-5582\(60\)90048-1](https://doi.org/10.1016/0029-5582(60)90048-1)
19. A. Scemama, M. Caffarel, A. Savin, Maximum probability domains from quantum Monte Carlo calculations. *J. Comput. Chem.* **28**, 442–454 (2007). <https://doi.org/10.1002/jcc.20526>
20. P.S.V. Kumar, V. Raghavendra, V. Subramanian, Bader's theory of atoms in molecules (AIM) and its applications to chemical bonding. *J. Chem. Sci.* **128**, 1527–1536 (2016). <https://doi.org/10.1007/s12039-016-1172-3>
21. F. Cortés-Guzmán, J.I. Rodríguez, J.S.M. Anderson, Chap. 1 - Introduction to QTAIM and beyond, in: J.I. Rodríguez, F. Cortés-Guzmán, J.S.M.B.T.-A. in Q.C.T.B.Q. Anderson (Eds.), (Elsevier, 2023), pp. 1–19. <https://doi.org/10.1016/B978-0-323-90891-7.00021-9>
22. T.A. Osswald, G. Menges, *Materials Science of Polymers for Engineers* (Carl Hanser Verlag GmbH & Company KG, 2012). <https://books.google.hu/books?id=RY9PAGAAQBAJ>
23. J. Joseph, E.D. Jemmis, Red-, Blue-, or no-shift in hydrogen bonds: a unified explanation. *J. Am. Chem. Soc.* **129**, 4620–4632 (2007). <https://doi.org/10.1021/ja067545z>
24. B. Liu, N. Vu-Bac, X. Zhuang, X. Fu, T. Rabczuk, Stochastic full-range multiscale modeling of thermal conductivity of polymeric carbon nanotubes composites: a machine learning approach.

- Compos. Struct. **289**, 115393 (2022). <https://doi.org/10.1016/j.compstruct.2022.115393>
25. B. Liu, W. Lu, T. Olofsson, X. Zhuang, T. Rabczuk, Stochastic interpretable machine learning based multiscale modeling in thermal conductivity of polymeric graphene-enhanced composites. *Compos. Struct.* **327**, 117601 (2024). <https://doi.org/10.1016/j.compstruct.2023.117601>
26. M.W. Schmidt, J. Ivanic, K. Ruedenberg, Covalent bonds are created by the drive of electron waves to lower their kinetic energy through expansion. *J. Chem. Phys.* **140**, 204104 (2014). <https://doi.org/10.1063/1.4875735>
27. A. Scemama, A. Savin, What is the number of electrons in a Spatial domain? (2022). <https://doi.org/10.48550/arXiv.2205.09365>
28. W. Jennings, A.G. *Chromatography*, (Elsevier Sci., 2012). <https://books.google.hu/books?id=UjwLljZXv3IC>
29. W. Feller, *An Introduction To Probability Theory and its Applications*, vol. 1 (Wiley, 1968). <https://books.google.hu/books?id=mfRQAAAAMAAJ>
30. G.A. Korn, T.M. Korn, *Mathematical Handbook for Scientists and Engineers: Definitions, Theorems, and Formulas for Reference and Review* (Dover, 2013). <https://books.google.hu/books?id=A4XCAgAAQBAJ>
31. J. Zar, Spearman rank correlation. *Encycl Biostat.* (2005). <https://doi.org/10.1002/0470011815.b2a15150>
32. Á. János, John Dobson; Georg Jansen; Tim Gould, Introduction, in: J. Ángyán, J. Dobson, G. Jansen, T. Gould (Eds.), *London Dispers. Forces Mol. Solids Nano-Structures An Introd. to Phys. Model. Comput. Methods*, R. Soc. Chem. 0 (2020). <https://doi.org/10.1039/9781782623861-00001>
33. D.M. Himmelblau, *Process Analysis by Statistical Methods* (John Wiley & Sons, Inc., New York, 1970)
34. P.I. Dergunov, A.V. Klinger, A.V. Tvardovskii, A.A. Fomkin, Use of the Lennard-jones potential in modeling the absorption deformation of microporous carbon adsorbents. *J. Eng. Phys. Thermophys.* **79**, 276–282 (2006). <https://doi.org/10.1007/s10891-006-0097-y>
35. S. Stephan, M. Thol, J. Vrabec, H. Hasse, Thermophysical properties of the Lennard-Jones fluid: database and data assessment. *J. Chem. Inf. Model.* **59**, 4248–4265 (2019). <https://doi.org/10.1021/acs.jcim.9b00620>
36. S. Stephan, U.K. Deiters, Characteristic curves of the Lennard-jones fluid. *Int. J. Thermophys.* **41**, 147 (2020). <https://doi.org/10.1007/s10765-020-02721-9>
37. X. Wang, S. Ramírez-Hinestrosa, J. Dobnikar, D. Frenkel, The lennard-jones potential: when (not) to use it. *Phys. Chem. Chem. Phys.* **22**, 10624–10633 (2020). <https://doi.org/10.1039/C9CP05445F>
38. K. Ohwada, On the Pauling electronegativity scales—II. *Polyhedron* **3**, 853–859 (1984). [https://doi.org/10.1016/S0277-5387\(00\)84634-3](https://doi.org/10.1016/S0277-5387(00)84634-3)
39. E.J.J. Little, M.M. Jones, A complete table of electronegativities. *J. Chem. Educ.* **37**, 231 (1960). <https://doi.org/10.1021/ed037p231>
40. E. Grushka, N. Grinberg (eds.), *Advances in Chromatography* (CRC, 2017). <https://doi.org/10.1201/9781315116372>
41. A.C. Legon, D.J. Millen, Angular geometries and other properties of hydrogen-bonded dimers: a simple electrostatic interpretation of the success of the electron-pair model. *Chem. Soc. Rev.* **16**, 467–498 (1987). <https://doi.org/10.1039/C9871600467>
42. M. Chaplin, Hydrogen bonding in Water, 1–9, (2022). https://water.lsbu.ac.uk/water/water_hydrogen_bonding.html/
43. P. McKeown, M.D. Jones, The chemical recycling of PLA: a review. *Sustain. Chem.* **1**, 1–22 (2020). <https://doi.org/10.3390/suschem1010001>

Publisher's note Springer Nature remains neutral with regard to jurisdictional claims in published maps and institutional affiliations.